Imaging Optical Fields Through Heavily Scattering Media

Jason A. Newman and Kevin J. Webb*
School of Electrical and Computer Engineering, Purdue University 465 Northwestern Avenue, West Lafayette, Indiana 47907-1285, USA
(Received 12 February 2014; published 30 December 2014)

Coherent imaging and communication through or within heavily scattering random media has been considered impossible due to the randomization of the information contained in the scattered electromagnetic field. We report a remarkable result based on speckle correlations over incident field position that demonstrates that the field incident on a heavily scattering random medium can be obtained using a method that is not restricted to weak scatter and is, in principle, independent of the thickness of the scattering medium. Natural motion can be exploited, and the approach can be extended to other geometries. The near-infrared optical results presented indicate that the approach is applicable to other frequency regimes, as well as other wave types. This work presents opportunities to enhance communication channel capacity in the large source and detector number regime, for a new method to view binary stars from Earth, and in biomedical applications.

DOI: 10.1103/PhysRevLett.113.263903 PACS numbers: 42.25.Dd, 05.40.−a, 41.20.Jb, 42.30.Ms

Random scatter can have a detrimental impact in science, medicine, and communication, limiting the use of traditional imaging, sensing, and signaling methods. While scatter can increase communication capacity [1] and provide security [2], severe multipath effects degrade wireless communication [3], tissue scatter inhibits deep coherent imaging [4], and atmospheric scatter obscures Earth-based astronomical telescopes [5]. Recent work on imaging through scattering media [6–8] is effective when the scatter is weak. For example, the memory effect results in incident wave vector information being retained in weakly scattered light, where the medium is very thin [8–10], limiting imaging to relatively transparent media [8]. Quasiballistic photon gating also becomes a signal-to-noise or integration time challenge beyond very weakly scattering media [6,11]. Interesting recent results showing the ability to focus light through randomly scattering media in both space and time also face challenges as scatter increases [7,12]. Such wavefront shaping using spatial light modulators essentially relies on mapping (directly or indirectly) the field transmission matrix of the random medium [7,12–14], which becomes more complex with increasing scatter and in many practical environments. Despite these challenges, coherent imaging continues to be an active research topic, and has been since the advent of the laser, due to its broad impact [15–19].

Here, we present an imaging method that is effective with heavily scattered light and allows one to reconstruct fields incident on a scattering random medium. Such field information was previously considered to be unavailable from optical intensity measurements, as would be obtained from a camera image of a speckle pattern. This work complements recent efforts to control and image light in scattering media [6–8,11,13,14] because it addresses the heavily scattering regime and provides an avenue to extend coherent control and imaging to more opaque randomly scattering media. In our method, illustrated in Fig. 1, speckle intensity images are taken as a function of object position and then used to calculate the spatial speckle intensity correlation. With sufficient scatter, meaning that the speckle field statistics are zero mean and circular Gaussian (indicated by a unity speckle intensity contrast ratio for coherent light) [20], the spatial speckle intensity correlation can be expressed using a moment theorem [21] as the magnitude squared of the electric field autocorrelation [22]. Under these conditions and over sufficiently small scan distances, resulting in a set of intensity images having constant mean, the spatial speckle intensity correlation is independent of the thickness and scattering properties of the random medium and depends solely on the incident electric field.

We use a Green's function representation for the electric field spatial autocorrelation at detector point $\mathbf{r}_d$ given by [22,23]

$$\begin{aligned}\langle E[U](\mathbf{r}_d)E^*[U(\Delta\mathbf{r})](\mathbf{r}_d)\rangle &= \left\langle \int d\mathbf{r}' U(\mathbf{r}')G(\mathbf{r}_d,\mathbf{r}') \right. \\ &\quad \left. \times \int d\mathbf{r}'' U^*(\mathbf{r}''+\Delta\mathbf{r})G^*(\mathbf{r}_d,\mathbf{r}''+\Delta\mathbf{r}) \right\rangle, \quad (1)\end{aligned}$$

where $U(\cdot)$ is the incident field, $E[U(\cdot)]$ is the speckle field at $\mathbf{r}_d$ due to the incident field $U(\cdot)$, $\Delta\mathbf{r}$ is a source translation vector, and $\langle\cdot\rangle$ is an average (mathematically, over scatterer position, but practically over a speckle image on a camera). The scan step magnitude, $|\Delta\mathbf{r}|$, is assumed to be large relative to the wavelength, making local correlations associated with, for example, the memory effect [9] negligible. With sufficient scatter, we therefore assume that contributions to the measured intensity correlation only occur from the joint support of the electric field and the offset electric field, and with stationary statistics and

after setting $P(\mathbf{r}_d,\Delta\mathbf{r}) = \langle G(\mathbf{r}_d,\mathbf{r}')G^*(\mathbf{r}_d,\mathbf{r}''+\Delta\mathbf{r})\rangle$ in (1), we find

$$\langle E[U](\mathbf{r}_d)E^*[U(\Delta\mathbf{r})](\mathbf{r}_d)\rangle = P(\mathbf{r}_d,\Delta\mathbf{r})\int d\mathbf{r}' U(\mathbf{r}')U^*(\mathbf{r}'+\Delta\mathbf{r}). \quad (2)$$

With heavy scatter or sufficiently small $\Delta\mathbf{r}$, still large relative to the wavelength, $P(\mathbf{r}_d,\Delta\mathbf{r})$ can be assumed constant. Under the assumption of zero-mean circular Gaussian fields, Reed's moment theorem [21] can be used to express the intensity autocorrelation as the magnitude squared of the electric field correlation, resulting in $\langle I[U]I^*[U(\Delta\mathbf{r})]\rangle = |\langle E[U]E^*[U(\Delta\mathbf{r})]\rangle|^2$. Using this result with (2), and with a normalization $\tilde{I}[U(\cdot)] = (I - \langle I\rangle)/\langle I\rangle$, we arrive at an estimate for the normalized intensity autocorrelation as

$$\langle \tilde{I}[U]\tilde{I}[U(\Delta\mathbf{r})]\rangle = \left|\int d\mathbf{r}' U(\mathbf{r}')U^*(\mathbf{r}'+\Delta\mathbf{r})\right|^2. \quad (3)$$

By rewriting the incident field autocorrelation in terms of its plane wave spectrum, (3) becomes

$$\langle \tilde{I}[U]\tilde{I}[U(\Delta\mathbf{r})]\rangle = |\mathcal{F}^{-1}\{|U(\mathbf{k}_\perp)|^2\}|^2, \quad (4)$$

where $\mathcal{F}^{-1}$ is the inverse Fourier transform and $\mathbf{k}_\perp$ is the Fourier conjugate variable of $\Delta\mathbf{r}$. We see that the spatial speckle intensity correlation is determined solely by the magnitude of the field's spatial Fourier transform. Considering the propagating plane wave spectrum, the result in (4) is insensitive to phase in the Fourier domain, leading to insensitivity to the object plane (incident field reference position) offset distance from the random medium [24].

Without any scatter, spatially scanning the incident field would simply yield the incident beam intensity autocorrelation, $\int d\mathbf{r}'|U(\mathbf{r}')|^2|U(\mathbf{r}'+\Delta\mathbf{r})|^2$. As scatter is introduced into the system, speckle forms. With increasing scatter, such that the statistics are fully developed (zero-mean and circular Gaussian) and the mean intensity is approximately constant over scan position, the spatial speckle intensity correlation approaches (4). Therefore, the spatial speckle intensity correlation is bounded between (4) and the incident field intensity autocorrelation. Given that (4) holds, it can be inverted with suitable data to determine the incident field, as we demonstrate.

Figure 1 shows the experiment. A patterned laser beam, the object of interest, is incident on a scattering slab, and a camera measures the transmitted speckle intensity. In our experiment, a narrow linewidth (< 10 MHz) laser beam from an 850 nm laser diode illuminated a set of apertures placed about 2 cm in front of the scattering slab. The laser beam and pattern shaping apertures were scanned across the randomly scattering slab in a raster pattern using two orthogonally mounted linear stages and associated mirrors. Two lenses were used in a 4-f configuration to spatially filter the speckle pattern along with a third lens to magnify

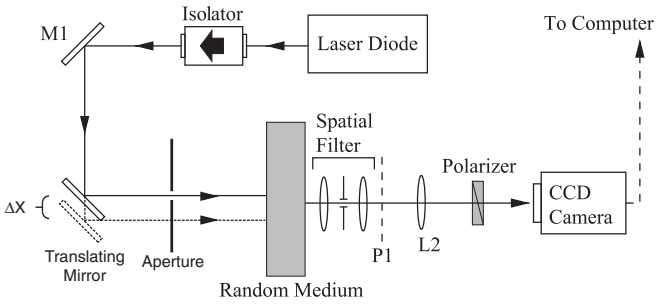

FIG. 1. Experimental setup. Scattering slabs with reduced scattering coefficients of 4 or 14 cm^{-1} and thicknesses of 3, 6, and 9 mm were illuminated by an 850 nm laser which was shaped by an aperture arrangement. The patterned beam, the object of interest, was scanned across the slab. The speckle imaging arrangement was composed of a CCD camera, a spatial filter, a magnification lens, and a polarizer. The measurement imaged a small spot on the back of the scattering slab, resulting in a mean intensity that was independent of position within the camera image. With heavy scatter, this mean is independent of the object position over sufficiently small scan distances, the case in this Letter.

an approximately 1 mm × 1 mm area on the randomly scattering slab, to ensure that the average speckle size was much larger than a single CCD pixel. A polarizer was used to image either the co- or cross-polarized speckle patterns, and the data presented here are for copolarized light. With sufficient scatter, the co- and cross-polarized speckle patterns yield identical correlations, and with increasing scatter, the cross-polarized spatial speckle correlation converges more rapidly to the heavy scatter result. At each scan position, the speckle intensity pattern was imaged using a 12-bit, 1392 by 1040 pixel CCD camera. Typically, a scanning step size of 25 μm and 150 steps were used in one dimension for the reconstructed incident field images that we present.

Figure 2 gives a comparison between our theory in (4), based on field correlations, the intensity correlation of the incident beam, and experimental speckle intensity correlations for slabs with a reduced scattering coefficient of $\mu_s' = 4\ \text{cm}^{-1}$ and thicknesses of 3, 6, and 9 mm, and $\mu_s' = 14\ \text{cm}^{-1}$ slabs with thicknesses of 3 and 6 mm. The material was a clear acrylic embedded with titanium dioxide scatterers with a mean diameter of 50 nm. The object was a single circular aperture in a black screen (diameter of 500 μm) illuminated by a quasispherical wave generated from the laser beam transmitted through a 50 μm diameter circular aperture placed 65 mm in front of it and farther from the scattering slab. The incident beam intensity autocorrelation in Fig. 2 gives the upper bound for the speckle intensity correlation. As the slab thickness increases, the speckle intensity correlation approaches the magnitude squared of the field correlation, as given by (3). With increasing slab thickness, the mean speckle intensity becomes nearly constant over incident field position. For the slabs with $\mu_s' = 4\ \text{cm}^{-1}$, a minimum thickness of 6 mm is required for a constant mean over the incident field scan

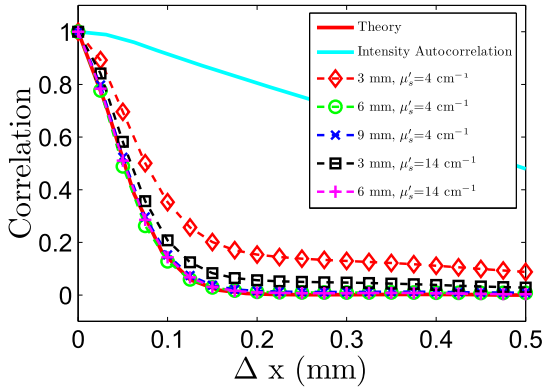

FIG. 2 (color online). Speckle spatial intensity correlation comparisons between our theory, the autocorrelation of the incident intensity, and experimental data, for scattering samples with a reduced scattering coefficient of $\mu_s' = 4$ cm^{-1} and thicknesses of 3, 6, and 9 mm, and $\mu_s' = 14$ cm^{-1} samples with thicknesses of 3 and 6 mm. As the scattering in the slab increases, the spatial speckle intensity correlation approaches the theory in (4).

distance we used. With the heavier scattering samples having $\mu_s' = 14$ cm^{-1}, the 3 mm thick slab already shows significant convergence to (4), and the 6 mm slab result is in excellent agreement with the theory. In general, the decorrelation rate of (4) becomes more rapid for smaller apertures, and is inversely related to the spatial Fourier spectral width of the incident beam, an observation of significance for communication information capacity [1].

For incident field reconstruction, we used a scattering slab of thickness 9 mm having $\mu_s' = 4$ cm^{-1}, again clear acrylic with 50 nm titanium dioxide scatterers. Using the measured spatial speckle intensity correlation, the incident field can be reconstructed through an inversion of (4), which can be written

$$U \simeq \mathcal{F}^{-1}\{[\mathcal{F}\{[\langle \tilde{I}[U]\tilde{I}[U(\Delta\mathbf{r})]\rangle]^{(1/2)} e^{i\phi_1(\Delta\mathbf{r})}\}]^{(1/2)} e^{i\phi_2(\mathbf{k}_\perp)}\}, \tag{5}$$

where there are two phase reconstructions necessary, ϕ_1 and ϕ_2, done in that sequence. For an arbitrary complex incident field, the spatial speckle field correlation, which is obtained through the reconstruction of ϕ_1, must have Hermitian symmetry (as it is the inverse Fourier transform of a real quantity, the magnitude squared of the field spectrum). If the incident field is real (with uniform phase) or has even symmetry (about two orthogonal directions in the plane of the slab), the field correlation must be both even and real, constraining ϕ_1 to values of either zero or π. Under this condition, ϕ_1 can be reconstructed using a simple continuity condition (at the zeros of the field magnitude). The reconstruction of ϕ_2 can be accomplished using an iterative phase retrieval algorithm [25]. Each iteration involved Fourier transforming between the real space and spatial frequency domains. In the frequency domain, the Fourier magnitude was replaced with the Fourier magnitude of (5) using the reconstruction of ϕ_1. In our reconstructions, the hybrid IO and error reduction methods were used to enforce spatial constraints during the field reconstruction [25–27]. The hybrid IO method was used for a couple of dozen successive iterations, followed by a single iteration using the error reduction method. This pattern was continued throughout the reconstruction process. Convergence was reached typically with several hundred iterations (total of error reduction plus hybrid IO).

In Fig. 3, we show a field reconstruction for a beam that was patterned using a set of circular apertures, where a 50 μm diameter aperture generated a quasispherical wave, and a 500 μm diameter aperture placed 65 mm in front of this and nearer to the scattering sample limited the field spatial support. The resulting patterned field has curvature in both magnitude and phase, as shown in Figs. 3(a) and 3(b), respectively. With this patterned beam incident on the scattering slab, copolarized speckle intensity images were collected as the patterned beam (laser beam plus apertures) was scanned. The resulting speckle images were used to calculate the spatial speckle intensity correlation, and (5) was then used to reconstruct the patterned beam field. In this case, the field magnitude had no zero crossings, so $\phi_1 = 0$. The iterative phase retrieval method with a tight spatial constraint using *a priori* information about the beam shaping aperture size was used to determine ϕ_2. The reconstruction results are shown in Figs. 3(c) and 3(d) as the reconstructed magnitude and phase, ϕ_2, respectively. Notice that the reconstructed phase agrees nicely with our numerically estimated incident field phase in the

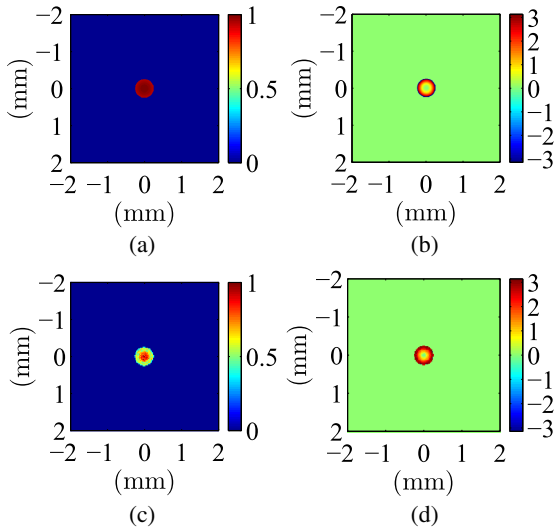

FIG. 3 (color online). Field reconstruction results for a 500 μm circular aperture. The circular aperture was illuminated with a quasispherical wave generated by a 50 μm circular aperture placed 65 mm in front of it. The scattering slab was 9 mm thick and had a reduced scattering coefficient of $\mu_s' = 4$ cm^{-1}. (a) Estimated aperture field magnitude. (b) Estimated aperture field phase. (c) Reconstructed field magnitude. (d) Reconstructed field phase. The phase images have been truncated to only show the phase where the magnitude is significant.

experiment, and that the reconstructed magnitude has more curvature than the numerical estimate. This magnitude smoothing is not due to truncation of the Fourier spectrum, and may be associated with small changes in the mean intensity as a function of scan position.

Using the same scattering medium as before (9 mm thick with $\mu_s' = 4$ cm^{-1}), an aperture arrangement consisting of two side by side 0.8 mm diameter circular holes separated by 1.6 mm, center to center, was placed in front of the laser beam. The numerically estimated magnitude and phase for the incident field are shown in Figs. 4(a) and 4(b), respectively. Again, using only the speckle intensity images, the intensity correlation in (4) was calculated. For the outer reconstruction in (5), ϕ_1 was assigned to values of zero or π by tracking the zero crossings. We used a much more relaxed spatial constraint for the ϕ_2 phase reconstruction, faintly seen in Fig. 4(c) as the large encompassing outer circle. We reconstructed ϕ_2 using iterative phase retrieval, as in the single hole experiment. The reconstruction results are shown in Figs. 4(c) and 4(d) as the reconstructed magnitude and phase, respectively. Again, the reconstructed phase conforms nicely to the numerically estimated phase, while the magnitude data show correctly separated holes with some smoothing around the edges of the two apertures. A random initial phase was assigned, and as iterations progressed, the holes formed and moved towards the right side of the spatial constraint region. Consequently, the reconstructed holes are positioned slightly to the right of center. This drift occurs due to the ambiguity of the phase reconstruction to linear phase (absolute positioning of the two holes in the transverse plane).

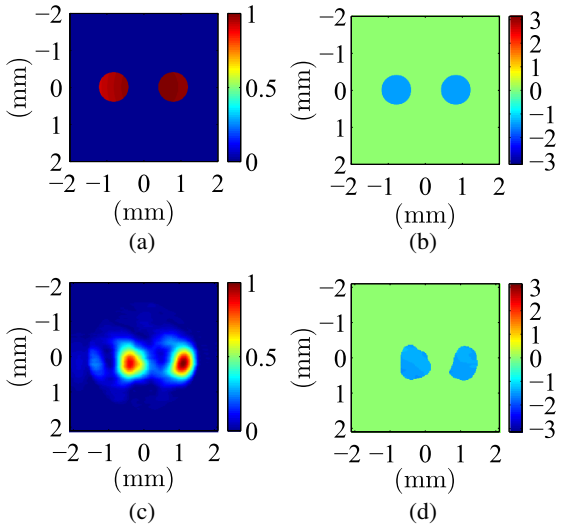

FIG. 4 (color online). Reconstructed field for a two-hole illumination pattern. The scattering slab was 9 mm thick and had a reduced scattering coefficient of $\mu_s' = 4$ cm^{-1}. (a) Estimated aperture field magnitude. (b) Estimated aperture field phase. (c) Reconstructed field magnitude. (d) Reconstructed field phase. The phase images have been truncated to only show the phase where the magnitude is significant.

The speckle memory effect can be used to image through scattering media, but is limited to an angular field of view inversely proportional to the thickness of the scattering medium, under the assumption that the illumination spot is wide [9]. It has proven effective in imaging experiments with thin scattering media [8], usually no more than a few tens of microns thick. The results presented here used a 9 mm thick heavily scattering slab, much thicker and more heavily scattering than what has been practical with the memory effect. In general, our method is independent of scattering thickness, given sufficient scatter. In the memory effect, as the angle of incidence of the source is changed, the imaged speckle pattern shifts [10]. Figure 5 shows the speckle image cross-correlation as a function of pixel offset for our data. As the object moves, the correlation peak remains centered above zero offset. This indicates that the speckle pattern is not shifting in response to the changing object position and that the results we achieved are unrelated to the memory effect.

Speckle images have been used to obtain information about objects using a method called speckle correlography imaging [28]. This method relies on information about the object being encoded into the speckle spots themselves. The primary difference from our method is that correlations are taken over individual speckle images, while our method uses correlations over object position. Another way of saying this is that our method uses an ensemble average of correlations over object position from individual detectors, while speckle correlography uses an ensemble average of correlations from speckle images. We show in Fig. 6 the ensemble average power spectrum from one of our two-hole aperture experiments. The radial symmetry of the power spectrum is a clear indication that information about the two hole illuminated aperture, which is not circularly symmetric, is not present in the power spectrum.

Earth-based astronomy is one important application of our speckle imaging technique. Fluctuations in the atmosphere's

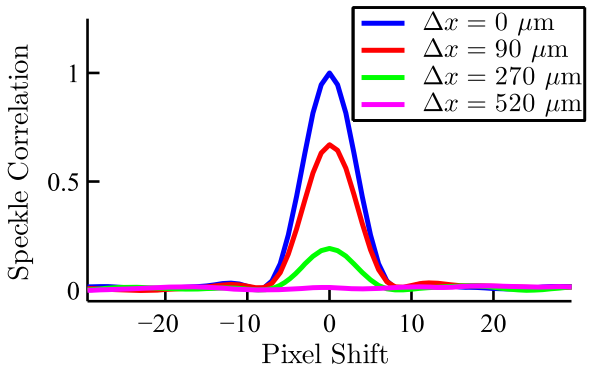

FIG. 5 (color online). Speckle image cross-correlation as a function of pixel shift for four different object positions. The illuminating object was a two hole aperture, aligned in the x direction. The maximum correlation is centered at zero, indicating that the speckle pattern is not translating in response to changes in the object position.

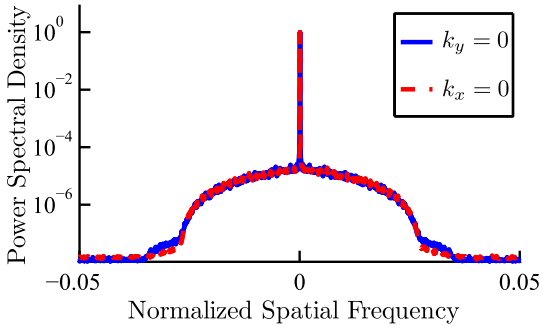

FIG. 6 (color online). Ensemble average power spectral density, averaged over 100 speckle images, shown on a log scale. The power spectral density, in this case, is practically circular, as shown by the cross sections at $k_{x,y} = 0$. The illuminating object was a two hole aperture, aligned in the x direction. The speckle image power spectral density clearly does not contain information about the object. In our experiments, the speckle image power spectrum is determined by the imaging optics; i.e., the detection optics dictate the speckle size and shape.

density cause speckled stellar images which significantly impact the observational capabilities of Earth-based telescopes. Consequently, some binary stars cannot be distinguished from single stars, which has led to signal processing methods such as speckle masking [29]. Our method, in conjunction with the Earth's rotation and atmospheric scatter, provides another approach. For example, assuming that the atmosphere can be considered stationary for 10 ms [5], commonly called the seeing time, star systems spanning up to 700 nrad (about 0.15 arcsec) can be imaged by our method. This means within the Milky Way there are hundreds of potential stars that could be imaged [30].

We have presented a method to image fields through scattering media like tissue that leads to an understanding of how to image moving objects and to control fields within the medium. Given sufficient scatter, the measured speckle correlations are independent of the material scattering properties and size. The method therefore provides coherent imaging potential in scattering regimes inaccessible to current methods. For example, the field of a sufficiently coherent guide star introduced into the scattering medium could be determined using our method, allowing the focusing of an external illumination to that point (for therapy, in a medical application) without the need for difficult optimization searches that ultimately require access to the guide star position [7]. Other implementations could permit the tracking and imaging of objects embedded deep within strongly scattering media. By extracting the incident field from intensity correlations over position, and measuring the scattered field using a spectral domain interferometer [31], the field Green's function for the random medium could be obtained. This itself provides spatial and temporal characterization information, and also allows direct control of the incident light to achieve an arbitrary pattern with the scattered light using, for example, a spatial light modulator.

This work was supported by the National Science Foundation (NSF) under Grants No. 0701749-ECCS and No. 1028610-ECCS.

*Corresponding author.
webb@purdue.edu

[1] A. L. Moustakas, H. U. Baranger, L. Balents, A. M. Sengupta, and S. H. Simon, Science **287**, 287 (2000).
[2] R. Pappu, B. Recht, J. Taylor, and N. Gershenfeld, Science **297**, 2026 (2002).
[3] S. M. Alamouti, IEEE J. Sel. Areas Commun. **16**, 1451 (1998).
[4] D. Huang, E. A. Swanson, C. P. Lin, J. S. Schuman, W. G. Stinson, W. Chang, M. R. Hee, T. Flotte, K. Gregory, C. A. Puliafito *et al.*, Science **254**, 1178 (1991).
[5] A. Tokovinin, Appl. Opt. **41**, 957 (2002).
[6] A. Velten, T. Willwacher, O. Gupta, A. Veeraraghavan, M. G. Bawendi, and R. Raskar, Nat. Commun. **3**, 745 (2012).
[7] O. Katz, E. Small, Y. Bromberg, and Y. Silberberg, Nat. Photonics **5**, 372 (2011).
[8] J. Bertolotti, E. G. van Putten, C. Blum, A. Lagendijk, W. Vos, and A. P. Mosk, Nature **491**, 232 (2012).
[9] S. Feng, C. Kane, P. A. Lee, and A. D. Stone, Phys. Rev. Lett. **61**, 834 (1988).
[10] I. Freund, M. Rosenbluh, and S. Feng, Phys. Rev. Lett. **61**, 2328 (1988).
[11] A. Kirmani, T. Hutchison, J. Davis, and R. Raskar, Int. J. Comput. Vis. **95**, 13 (2011).
[12] I. M. Vellekoop and A. P. Mosk, Opt. Lett. **32**, 2309 (2007).
[13] T. Kohlgraf-Owens and A. Dogariu, Opt. Express **16**, 13225 (2008).
[14] S. Popoff, G. Lerosey, M. Fink, A. C. Boccara, and S. Gigan, Nat. Commun. **1**, 81 (2010).
[15] E. N. Leith and J. Upatnieks, J. Opt. Soc. Am. **56**, 523 (1966).
[16] P. S. Idell, J. R. Fienup, and R. S. Goodman, Opt. Lett. **12**, 858 (1987).
[17] I. Freund, Phys. Lett. A **147**, 502 (1990).
[18] J. D. McKinney, M. A. Webster, K. J. Webb, and A. M. Weiner, Opt. Lett. **25**, 4 (2000).
[19] A. K. Dunn, H. Bolay, M. A. Moskowitz, and D. A. Boas, J. Cereb. Blood Flow Metab. **21**, 195 (2001).
[20] J. W. Goodman, *Statistical Optics* (Wiley-Interscience, New York, 1985).
[21] I. S. Reed, IRE Trans. Inf. Theory **8**, 194 (1962).
[22] J. A. Newman and K. J. Webb, Opt. Lett. **37**, 1136 (2012).
[23] Z. Wang, K. J. Webb, and A. M. Weiner, Appl. Opt. **49**, 5899 (2010).
[24] J. W. Goodman, *Introduction to Fourier Optics* (McGraw-Hill, New York, 1968).
[25] J. R. Fienup, J. Opt. Soc. Am. A **4**, 118 (1987).
[26] R. P. Millane, J. Opt. Soc. Am. A **13**, 725 (1996).
[27] S. Marchesini, Rev. Sci. Instrum. **78**, 011301 (2007).
[28] J. W. Goodman, *Speckle Phenomena in Optics: Theory and Applications* (Roberts and Company Publishers, Greenwood Village, Colorado, 2007).
[29] G. P. Weigelt, Opt. Commun. **21**, 55 (1977).
[30] C. J. Lada, Astrophys. J. Lett. **640**, L63 (2006).
[31] M. A. Webster, T. D. Gerke, A. M. Weiner, and K. J. Webb, Opt. Lett. **29**, 1491 (2004).